

Article

Inexpensive *Ipomoea aquatica* Biomass-Modified Carbon Black as an Active Pt-Free Electrocatalyst for Oxygen Reduction Reaction in an Alkaline Medium

Yaqiong Zhang ¹, Chaozhong Guo ^{1,2}, Zili Ma ¹, Huijuan Wu ¹ and Changguo Chen ^{1,*}

Received: 13 July 2015 ; Accepted: 26 August 2015 ; Published: 25 September 2015

Academic Editor: Alina M. Balu

¹ College of Chemistry and Chemical Engineering, Chongqing University, Chongqing 400044, China; 20121802076@cqu.edu.cn (Y.Z.); czguo@cqw.edu.cn (C.G.); mzl@cqu.edu.cn (Z.M.); 20131802094@cqu.edu.cn (H.W.)

² Research Institute for New Materials Technology, Chongqing University of Arts and Sciences, Chongqing 402160, China

* Correspondence: cgchen@cqu.edu.cn; Tel./Fax: +86-23-6510-6053

Abstract: The development of inexpensive and active Pt-free catalysts as an alternative to Pt-based catalysts for oxygen reduction reaction (ORR) is an essential prerequisite for fuel cell commercialization. In this paper, we report a strategy for the design of a new Fe–N/C electrocatalyst derived from the co-pyrolysis of *Ipomoea aquatica* biomass, carbon black (Vulcan XC-72R) and FeCl₃·6H₂O at 900 °C under nitrogen atmosphere. Electrochemical results show that the Fe–N/C catalyst exhibits higher electrocatalytic activity for ORR, longer durability and higher tolerance to methanol compared to a commercial Pt/C catalyst (40 wt %) in an alkaline medium. In particular, Fe–N/C presents an onset potential of 0.05 V (*vs.* Hg/HgO) for ORR in an alkaline medium, with an electron transfer number (*n*) of ~3.90, which is close to that of Pt/C. Our results confirm that the catalyst derived from *I. aquatica* and carbon black is a promising non-noble metal catalyst as an alternative to commercial Pt/C catalysts.

Keywords: oxygen reduction reaction; Pt-free; *Ipomoea aquatic*; biomass

1. Introduction

Several studies have aimed to discover a large reserve of renewable and environment-friendly alternative energy sources, because of worsened environmental pollution and energy shortage. Fuel cells (FCs) are novel efficient, reliable, environment-friendly and flexible electric power generators, which can directly convert chemical energy into electrical energy with high conversion efficiency. The products of FC power generators, namely carbon dioxide and water, are nonhazardous to the environment. However, these power generators present slow kinetics of the cathodic oxygen reduction reaction (ORR) and therefore require the use of catalysts. Currently, the most effective and widely-used ORR electrocatalysts are those based on Pt. Nevertheless, Pt-based electrocatalysts are expensive and present poor methanol tolerance and low abundance, thereby hindering their commercialization [1–5]. In this regard, non-noble electrocatalysts with good catalytic activity, excellent methanol tolerance and high yield for FCs must be explored to replace Pt-based catalysts [6–9].

In 1964, Jasinski [10] reported that the transition metal macrocyclic cobalt phthalocyanine exhibits electrocatalytic activity for ORR. Since then, N-containing transition metal macrocyclic compounds have attracted considerable attention as promising alternatives to Pt-based ORR catalysts in FCs. Several scientists have investigated the oxygen-reduction catalytic activity of inexpensive

electrocatalysts by using different N-containing carbon materials as effective precursors [11–13]. These carbon materials include crude biomass, such as hemin [14–18], *Typha orientalis* [19], monkey grass [20], soybeans [21] and soya milk [22], which have attracted considerable interest, because they are abundant, environment friendly and inexpensive [23–27]. All of these studies have focused on using natural porphyrinato complexes containing hemin, *T. orientalis* and monkey grass to form catalytic sites.

Ipomoea aquatica, commonly known as swamp morning glory, is a widely-cultivated vegetable in the rural area of southern China. *I. aquatica* leaves contain abundant chlorophyll and Mg porphyrins, and the latter can be used as a precursor for the development of inexpensive ORR catalysts.

In this work, Fe–N/C catalyst was synthesized through a simple and readily-scalable approach by using *I. aquatica* leaves as the precursor. This approach comprises facile acid leaching and post-treatment in nitrogen gas (N₂) with Fe salts and carriers. The fabricated Fe–N/C catalyst exhibits excellent catalytic activity and 4e-pathway selectivity toward ORR, durability and methanol tolerance in an alkaline medium.

2. Experimental Section

2.1. Chemicals and Reagents

All of the reagents were of analytical grade and used without further purification. *I. aquatica* was obtained from a vegetable market in Chongqing, China, and was washed with distilled water before crushing. N₂ (99.9%) was purchased from Shang Yuan Company (Chongqing, China). Carbon black (Vulcan XC-72R) was acquired from Cabot® (Cabot Corporation, Boston, MA, USA). Commercially available 40 wt % Pt/C catalyst (JM Pt/C 40 wt %) was purchased from Johnson Matthey Corp (Yantai, China).

2.2. Catalyst Preparation

Typically, fresh leaves of *I. aquatica* (hereafter IA) were initially washed and dried at 90 °C for 36 h. The dried leaves were subsequently ground into powder and used as a starting material. The dried leaf powder was mixed with 80 mL of 0.5 M H₂SO₄ (Gai Tang Chemical Co., Ltd., Chengdu, China), and the obtained suspension was stirred and etched for 12 h. The product (denoted as *Ipomoea aquatica* after acid etching (IAA)) was then collected by centrifugation at 4500 rpm for 20 min to remove large-sized products and then dried at 90 °C for 9 h.

Briefly, 0.1 g of IAA was mixed with carbon black support (at a mass ratio of 1:1) and FeCl₃·6H₂O (Zhiyuan Chemical Products Co., Ltd., Zhengzhou, China) through ball milling for 30 min. The obtained substance (Fe–N/C) was treated in flowing N₂ at 900 °C for 2 h.

For control, Fe–N/C was subjected to acid leaching using 5 M H₂SO₄ (Gai Tang Chemical Co., Ltd., Chengdu, China) solution at room temperature for 24 h. The as-prepared sample was marked as N/C (Fe). N/C was obtained through heat treatment of IAA and the carbon black support at the same mass ratio without FeCl₃·6H₂O.

2.3. Characterization

Electrochemical measurements were conducted on a CHI 660 electrochemical workstation (CH Instruments, Austin, TX, USA), with a common three-electrode electrochemical cell. A platinum wire and an Hg/HgO (1 M KOH (Heng Aode Technology Co., Ltd., Beijing, China)) electrode were used as counter and reference electrodes, respectively. A rotating disk electrode (RDE) with a glassy carbon (GC) electrode (5-mm diameter, Tianjing Lanlike Electrochemical Instruments, Tianjin, China) coated with catalyst ink was used as a working electrode. Typically, 10 µL of the catalyst suspension dispersed in 0.5 wt % Nafion/isopropanol solution (DuPont, Wilmington, DE, USA) were dropped onto the pre-polished GC disk surface and then dried at room temperature. Sample loading is *ca.* 10 mg·cm^{−2}, and the mass loading of the commercial Pt/C-modified electrode is 5 mg·cm^{−2}.

All RDE experiments for ORR were performed within -0.7 to 0.3 V (*vs.* HgO/Hg) at a scan rate of $5 \text{ mV} \cdot \text{s}^{-1}$ in O_2 -saturated 0.1 M KOH solution.

X-ray photoelectron spectra (XPS) were obtained with a VG Escalab220 iXL spectrometer (VG Scientific, St Leonards-on-Sea, UK) fitted with an Al $K\alpha$ ($h\nu = 1486.69 \text{ eV}$) X-ray source to investigate surface composition and chemical status of the catalyst. X-ray diffraction (XRD) analysis was also conducted using a Shimadzu XRD-6000 X-ray diffractometer (Shimadzu, Kyoto, Japan) with Cu $K\alpha_1$ radiation ($\lambda = 1.54178 \text{ \AA}$) at scan rate of 4° min^{-1} .

3. Results and Discussion

The electrocatalytic activities of N/C, Fe–N/C and N/C (Fe) for ORR in 0.1 M KOH solution saturated with O_2 , as well as Fe–N/C in N_2 -saturated 0.1 M KOH solution, are shown in Figure 1. The onset potential (E_{onset}) and peak potential (E_p) are used to evaluate the electrocatalytic activities of the samples. In the figure, the linear sweep voltammograms (LSVs) of N/C, Fe–N/C and N/C (Fe) in O_2 -saturated solution present well-defined cathodic peaks. Fe–N/C exhibits the highest positive E_{onset} and E_p values over N/C and N/C (Fe), and is thus regarded as the sample with the highest electrocatalytic activity. However, no characteristic peak curves are present in the LSV of Fe–N/C in N_2 -saturated 0.1 M KOH solution, which demonstrates the excellent electrocatalytic activity of Fe–N/C toward ORR.

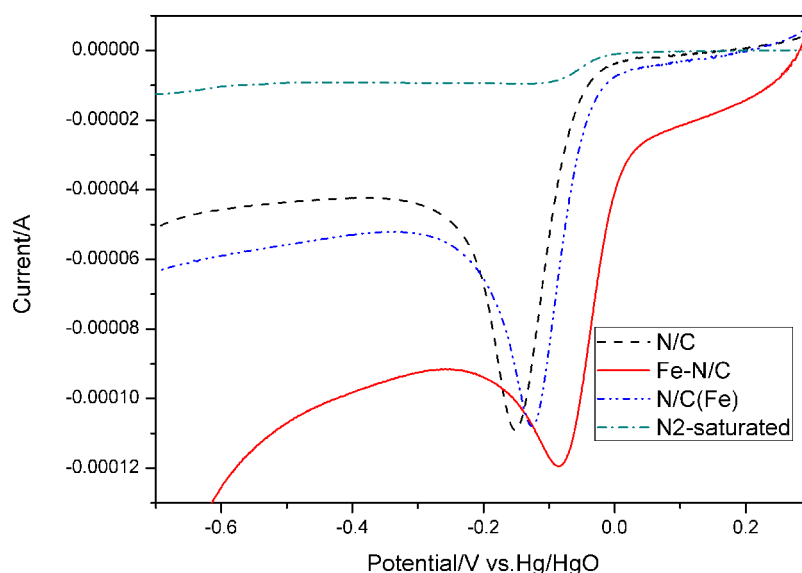


Figure 1. Linear sweep voltammograms of N/C, Fe–N/C and N/C (Fe) at a scan rate of $50 \text{ mV} \cdot \text{s}^{-1}$ in O_2 - and N_2 -saturated 0.1 M KOH solutions.

The catalyst Fe–N/C exhibits higher catalytic activity than N/C because of the participation of Fe in the heat treatment. To investigate whether or not Fe is an integral part of the active site in the catalyst, we determined the catalytic activity of N/C and N/C (Fe). Metal elements do not participate in the preparation of N/C, whereas Fe is involved at the beginning of the pyrolysis of N/C (Fe), but soaked in acid after the process. The E_{onset} and E_p values of N/C (Fe) are similar to those of N/C, but shift negatively relative to those of Fe–N/C upon soaking out of Fe. These results indicate that Fe is an integral part of the efficient ORR catalyst, and Fe–N/C exhibits the highest electrocatalytic activity among the sample catalysts.

RDE measurements were performed under different rotation rates to investigate the electrocatalytic mechanism of catalyst Fe–N/C for ORR and to determine the dominant processes in the alkaline medium (0.1 M KOH). Figure 2a shows that the current density on the Fe–N/C electrode increases with increasing rotation speed (from 400 to 2500 rpm). The overall number of transferred

electrons per oxygen molecule (n) involved in the ORR process is determined by the Koutecky–Levich (K–L) Equation [26]:

$$\frac{1}{j_d} = \frac{1}{j_k} + \frac{1}{0.62nFC_0D_O^{2/3}\nu^{-1/6}\omega^{1/2}} \quad (1)$$

where j_d is the diffusion-limited current density, j_k is the kinetic current density of the ORR, F is the Faraday constant ($96,485 \text{ C} \cdot \text{mol}^{-1}$), C_0 is the O_2 saturation concentration in the aqueous solution ($1.2 \times 10^{-6} \text{ mol} \cdot \text{cm}^{-3}$), D_0 is the O_2 diffusion coefficient in 0.1 M KOH electrolyte ($1.9 \times 10^{-5} \text{ cm}^2 \cdot \text{s}^{-1}$), ν is the kinetic viscosity of the solution ($0.01 \text{ cm}^2 \cdot \text{s}^{-1}$) and ω is the electrode rotation rate (rpm). Figure 2b shows the K–L plot of j_d^{-1} vs. $\omega^{-1/2}$ for Fe–N/C.

The parallelism and linearity of the K–L plots indicate consistent electron transfer across different potentials and first-order reaction kinetics with respect to the dissolved oxygen concentration [28]. The n value for ORR of Fe–N/C is ~ 3.90 from -0.5 to -0.7 V vs. that of the HgO/Hg electrode. The obtained value is considerably close to four, which is the n value for the ORR of commercial Pt/C. ORR catalyzed by Fe–N/C involves a mixture of two- and four-electron transfer pathways, but is dominated by the latter to mainly produce H_2O . O_2 reduction via the 4e-pathway is highly desirable to obtain maximum energy capacity. These results prove that Fe–N/C is a suitable alternative cathodic catalyst to commercial Pt-based catalysts for FC applications with reduced cost.

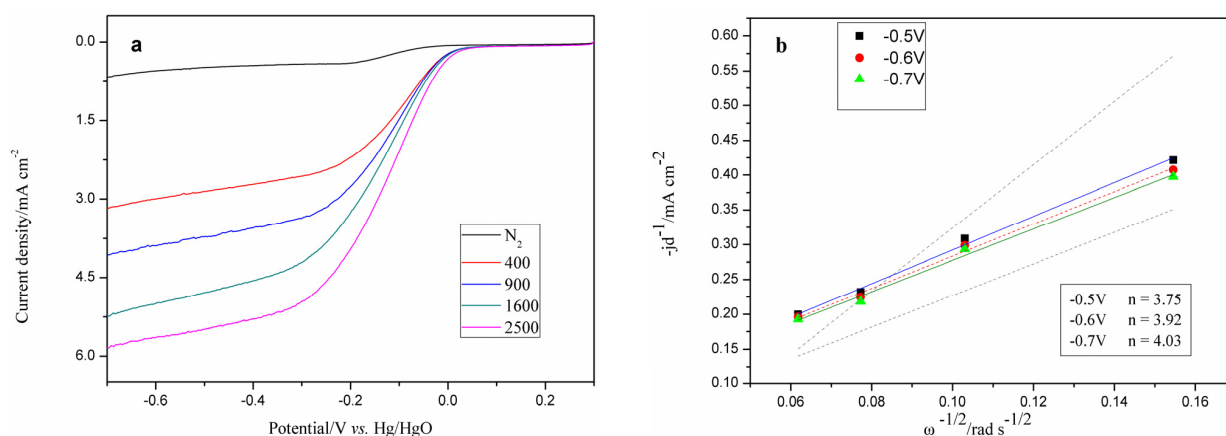


Figure 2. (a) Rotating disk electrode (RDE) voltammograms of the Fe–N/C electrode in O_2 -saturated 0.1 M KOH under different rotation rates at a scan rate of $5 \text{ mV} \cdot \text{s}^{-1}$. (b) Koutecky–Levich plots of the Fe–N/C electrode at different potentials.

The catalyst Fe–N/C exhibits excellent electrocatalytic activity with positive E_{onset} and E_p values for ORR. Nevertheless, stability and immunity toward methanol crossover are also required for practical applications. Pt-based catalysts demonstrate low stability and poor immunity toward methanol crossover. These limitations hindered the use of Pt-based catalysts in FCs [29].

The long-term stability of the Fe–N/C electrocatalyst was evaluated using an accelerated aging test (AAT) by continuous scanning 2000 cycles at a scan rate of $100 \text{ mV} \cdot \text{s}^{-1}$ and a potential range of -0.7 to 0.3 V (vs. Hg/HgO) in O_2 -saturated 0.1 M KOH solution. The ORR performance of Fe–N/C before and after AAT was assessed using the same three-electrode cell described in Section 2.3. For comparison, the stability of the JM Pt/C 40 wt % catalyst was also measured and is shown in the inset of Figure 3. The E_{onset} and half-wave peak (E_{hw}) negatively shift by 9 and 13 mV at the Fe–N/C-coated electrode after AAT relative to those before AAT. Moreover, the E_{onset} and E_{hw} of the JM Pt/C 40 wt % catalyst negatively shift by 54 and 36 mV under the same condition. Thus, the catalyst Fe–N/C exhibits higher stability than JM Pt/C 40 wt %.

As shown in Figure 4, the catalyst JM Pt/C 40 wt % and Fe–N/C catalysts show an obvious cathodic current response upon the introduction of O_2 into 0.1 M KOH solution. By contrast,

a different phenomenon occurs when 5.0 M methanol (Chuangdong Chemical Industry Co., Ltd., Chongqing, China) was added. The amperometric response of catalyst Fe–N/C remains stable with increasing amounts of methanol added to the solution at a time interval of 200 s. Meanwhile, catalyst JM Pt/C 40 wt % demonstrates a step-down decrease in cathodic current response with successive addition of methanol. These results confirm that the Fe–N/C catalyst exhibits significantly satisfactory immunity toward methanol.

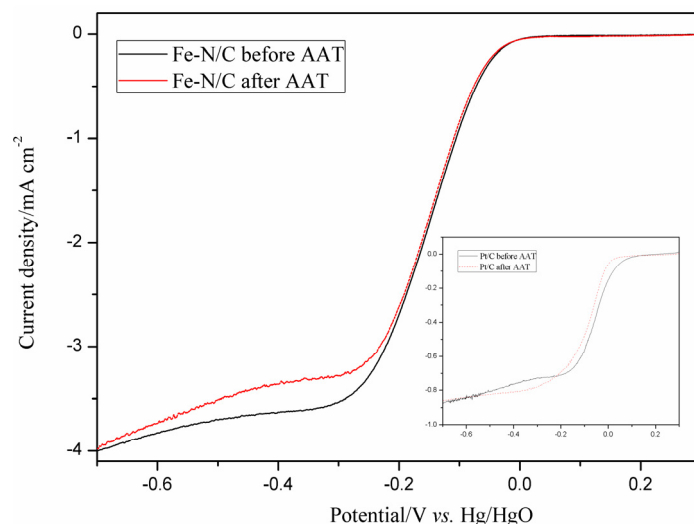


Figure 3. Oxygen reduction reaction (ORR) polarization curves for Fe–N/C and Pt/C (inset) before and after the accelerated aging test (AAT) in 0.1 M KOH solution at 1600 rpm.

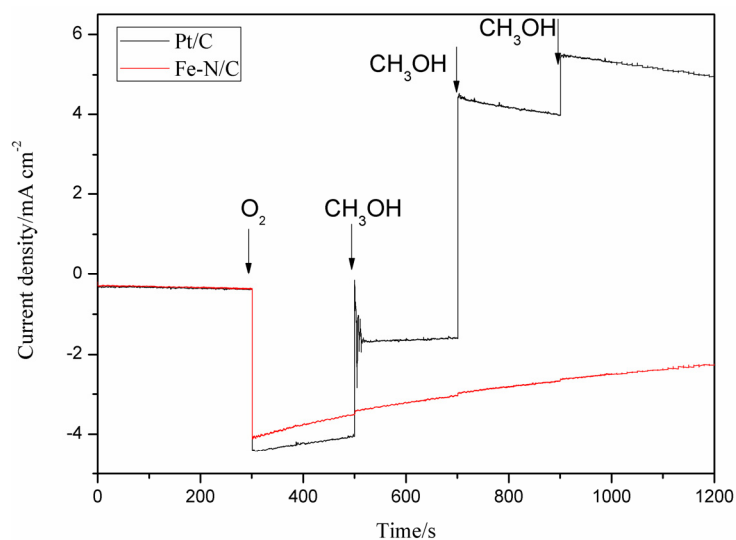


Figure 4. Amperometric current-time curves of Fe–N/C and Pt/C in N₂-saturated 0.1 M KOH solution under magnetic stirring (600 rpm) and N₂-protection from 0 to 300 s, followed by immediate introduction of O₂. The applied potential is –0.1 V. The arrows indicate the sequential addition of 5.0 M methanol.

Although catalyst Fe–N/C also exhibits slightly higher overpotential toward ORR than commercial catalyst JM Pt/C 40 wt %, the former contains an electron transfer number (*n*) similar to that of Pt/C and presents high tolerance to methanol and stability; hence, catalyst Fe–N/C

can be used as an alternative active ORR catalyst with considerable potential for FC and metal-air battery applications.

Figure 5 shows the XRD patterns of the three catalyst samples. The diffraction peaks at $2\theta = 25^\circ$ and 44° corresponds to the (002) and (101) planes of carbon, respectively. A crystal peak in catalyst Fe-N/C may be due to the incorporation of $\text{FeCl}_3 \cdot 6\text{H}_2\text{O}$. The XRD test results of the three samples show that adding $\text{FeCl}_3 \cdot 6\text{H}_2\text{O}$ significantly affects the structure of the catalyst. Nevertheless, no diffraction peaks for Fe are found in catalyst N/C (Fe), which indicates that this element is mostly removed through acid leaching.

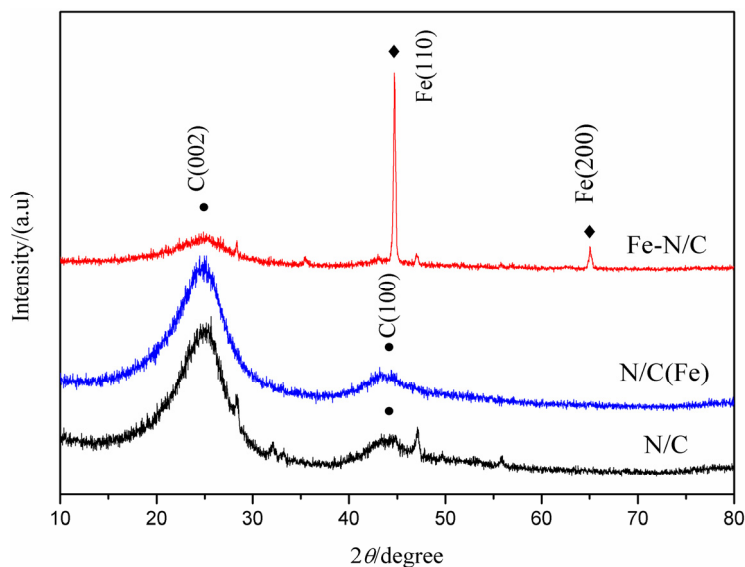


Figure 5. XRD patterns of N/C, Fe-N/C and N/C (Fe).

The XPS measurements of the three catalysts were conducted to investigate surface composition and chemical status of the catalysts, and the results are shown in Figure 6. The XPS survey spectra of catalyst N/C, Fe-N/C and N/C (Fe) (Figure 6a) show C1s, O1s, N1s, and less noticeable Fe2p signals (in Fe-N/C). Fe was not detected by XPS; nevertheless, this element could not be considered as absent from the material surface, because the XPS technique cannot accurately detect the presence of Fe because of its limited detection depth.

The C1s high-resolution spectra of the products are slightly asymmetric, as shown in Figure 6b. Each spectrum can be deconvoluted into two peaks, with a dominant peak at 284.5 eV and a small peak at 285.5 eV. The dominant peak is attributed to the sp^2 -hybridized C–C bond, and the small peak indicates the existence of functional groups, such as C–OH [30] and C–N configurations [20,31].

In the complex N1s high-resolution spectra (Figure 6c), pyridinic-N, Fe-N_x, pyrrolic-N and oxidized pyridinic-N species are clearly doped. The peak at 398.6 ± 0.2 eV corresponds to pyridinic-N species, whereas that at 399.6 ± 0.2 eV is speculated as Fe-N_x [32–34]; meanwhile, the peak at 400.8 ± 0.1 eV is ascribed to the pyrrolic-N structure [32,34], and that at 402–405 eV is due to oxidized pyridinic-N(N⁺–O[–]) species [32,33,35–37].

The appearance of the Fe-N_x characteristic peak further verifies that the catalyst comprises Fe. With the high levels of Fe-N_x and good ORR activity of Fe-N/C as bases, the following may be assumed: (1) N and Fe may have contributed to the excellent activity in alkaline solutions; and (2) Fe-N_x may be an effective active site. Furthermore, the N/C (Fe) sample exhibits slightly higher ORR activity than N/C, and the content of pyrrolic-N in N/C (Fe) is higher than that in N/C (Table 1); therefore, we could deduce that pyrrolic-N may be responsible for ORR activity.

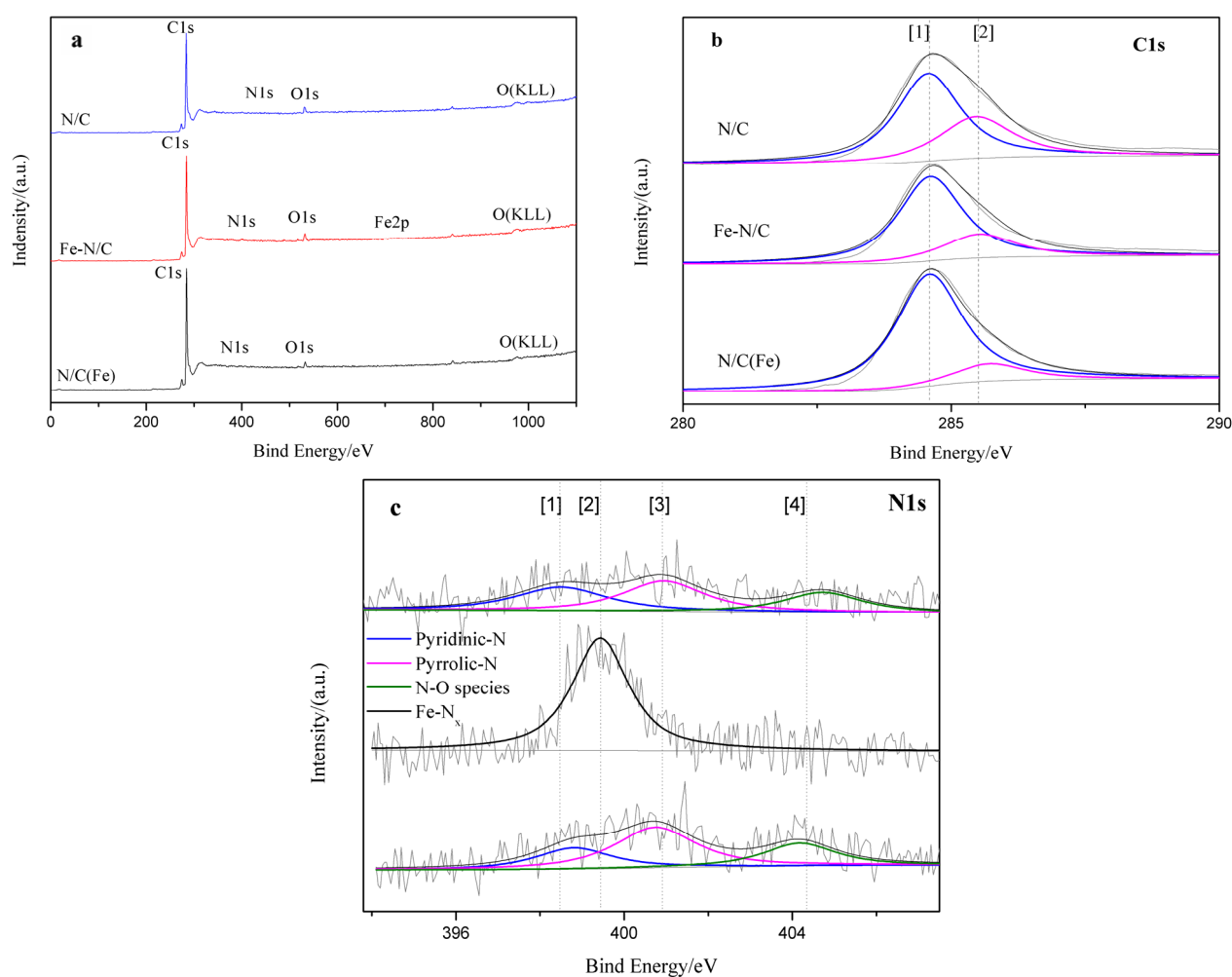


Figure 6. (a) XPS survey spectra of N/C, Fe-N/C and N/C (Fe). (b) XPS spectra of C1s of N/C, Fe-N/C and N/C (Fe). (c) XPS spectra of N1s of N/C, Fe-N/C and N/C (Fe).

Table 1. Peak positions, areas, full widths at half maximum (FWHM) and concentrations of N1s species in N/C, Fe-N/C and N/C (Fe) obtained from the XPS results.

Catalyst	Peak	Area	FWHM	Content
N/C	398.497 eV	803	2.600 eV	35%
	400.936 eV	909	2.300 eV	40%
	404.734 eV	567	2.200 eV	25%
Fe-N/C	399.436 eV	2328	1.603 eV	100%
N/C(Fe)	398.803 eV	599	2.167 eV	25%
	400.743 eV	12159	2.304 eV	50%
	404.173 eV	612	2.050 eV	25%

4. Conclusions

Fe-N/C is synthesized through the co-pyrolysis of *I. aquatica* leaves, carbon black (Vulcan XC-72R) and $\text{FeCl}_3 \cdot 6\text{H}_2\text{O}$ under nitrogen atmosphere. Fe is an integral part of the active Fe-N/C catalyst site. Electrochemical results show that Fe-N/C is an active catalyst with a four-electron transfer pathway toward ORR and with good stability and immunity toward methanol crossover. All

of the results have proven that the Fe–N/C catalyst can be a promising electrocatalyst with significant practical value.

Acknowledgments: This work was financially supported by the Natural Science Fund of China (NSFC21273292), the Basic and Frontier Research Program of Chongqing Municipality (CSTC2014jcyjA50038) and the Talent Introduction Project of Chongqing University of Arts and Sciences (R2014CJ02).

Author Contributions: Yaqiong Zhang contributed significantly to analysis and manuscript preparation, Also performed the data analyses and wrote the manuscript; Chaozhong Guo provided help in revising the manuscript. Huijuan Wu and Zili Ma contributed to the conception of the study. Changguo Chen helped perform the analysis with constructive discussions.

Conflicts of Interest: The authors declare no conflict of interest.

References

1. Lim, B.; Jiang, M.; Camargo, P.H.C.; Cho, E.C.; Tao, J.; Lu, X.; Zhu, Y.; Xia, Y. Pd-Pt bimetallic nanodendrites with high activity for oxygen reduction. *Science* **2009**, *324*, 1302–1305. [[CrossRef](#)] [[PubMed](#)]
2. Morozan, A.; Jégou, P.; Jusselme, B.; Palacin, S. Electrochemical performance of annealed cobalt–benzotriazole/CNTs catalysts towards the oxygen reduction reaction. *Phys. Chem. Chem. Phys.* **2011**, *13*, 21600–21607. [[CrossRef](#)] [[PubMed](#)]
3. Bashyam, R.; Zelenay, P. A class of non-precious metal composite catalysts for fuel cells. *Nature* **2006**, *443*, 63–66. [[CrossRef](#)] [[PubMed](#)]
4. Guo, C.Z.; Liao, W.L.; Sun, L.T.; Chen, C.G. Synthesis of non-noble nitrogen-containing catalysts for cathodic oxygen reduction reaction: A critical review. *Int. J. Electrochem. Sci.* **2015**, *10*, 2467–2477.
5. Poh, C.K.; Lim, S.H.; Tian, Z.; Lai, L.; Feng, Y.P.; Shen, Z.; Lin, J. Pt-W_xC nano-composites as an efficient electrochemical catalyst for oxygen reduction reaction. *Nano Energy* **2013**, *2*, 28–39.
6. Zheng, Y.; Jiao, Y.; Jaroniec, M.; Jin, Y.; Qiao, S.Z. Nanostructured metal-free electrochemical catalysts for highly efficient oxygen reduction. *Small* **2012**, *8*, 3550–3566. [[CrossRef](#)] [[PubMed](#)]
7. Guo, C.Z.; Chen, C.G.; Luo, Z.L. A novel nitrogen-containing electrocatalyst for oxygen reduction reaction from blood protein pyrolysis. *J. Power Sour.* **2014**, *245*, 841–845. [[CrossRef](#)]
8. Nabaie, Y.; Kuang, Y.; Chokai, M.; Ichihara, T.; Isoda, A.; Hayakawa, T.; Aoki, T. High performance Pt-free cathode catalysts for polymer electrolyte membrane fuel cells prepared from widely available chemicals. *J. Mater. Chem. A* **2014**, *2*, 11561–11564. [[CrossRef](#)]
9. Strickland, K.; Miner, E.; Jia, Q.; Tylus, U.; Ramaswamy, N.; Liang, W.; Sougrati, M.-T.; Jaouen, F.; Mukerjee, S. Highly active oxygen reduction non-platinum group metal electrocatalyst without direct metal-nitrogen coordination. *Nature Commun.* **2015**, *6*. [[CrossRef](#)] [[PubMed](#)]
10. Jasinski, R. A new fuel cell cathode catalyst. *Nature* **1964**, *201*, 1212–1213. [[CrossRef](#)]
11. Wang, K.; Wang, H.; Ji, S.; Feng, H.; Linkov, V.; Wang, R. Biomass-derived activated carbon as high-performance non-precious electrocatalyst for oxygen reduction. *RSC Adv.* **2013**, *3*, 12039–12042. [[CrossRef](#)]
12. Si, Y.J.; Chen, C.G.; Yin, W.; Cai, H. Electrocatalytic activity of non-precious metal catalyst Co–N/C toward oxygen reduction reaction. *Chin. Chem. Lett.* **2010**, *21*, 983–986. [[CrossRef](#)]
13. Guo, C.; Liao, W.; Li, Z.; Chen, C. Exploration of the catalytically active site structures of animal biomass-modified on cheap carbon nanospheres for oxygen reduction reaction with high activity, stability and methanol-tolerant performance in alkaline medium. *Carbon* **2015**, *85*, 279–288. [[CrossRef](#)]
14. Guo, C.Z.; Chen, C.G.; Luo, Z.L. The structural changes of blood pyropolymers and their beneficial electrocatalytic activity toward oxygen reduction. *Chin. Sci. Bull.* **2013**, *58*, 3698–3703. [[CrossRef](#)]
15. Maruyama, J.; Fukui, N.; Kawaguchi, M.; Abe, I. Application of nitrogen-rich amino acids to active site generation in oxygen reduction catalyst. *J. Power Sour.* **2008**, *182*, 489–495. [[CrossRef](#)]
16. Wang, Q.; Zhou, Z.Y.; Chen, D.J.; Lin, J.L.; Ke, F.S.; Xu, G.L.; Sun, S.G. Study of pyrolyzed hemin/C as non-platinum cathodic catalyst for direct methanol fuel cells. *Sci. China Chem.* **2010**, *53*, 2057–2062. [[CrossRef](#)]
17. Jiang, R.; Tran, D.T.; McClure, J.; Chu, D. Heat-treated hemin supported on graphene nanoplatelets for the oxygen reduction reaction. *Electrochem. Commun.* **2012**, *19*, 73–76. [[CrossRef](#)]

18. Xi, P.B.; Liang, Z.X.; Liao, S.J. Stability of hemin/C electrocatalyst for oxygen reduction reaction. *Int. J. Hydrog. Energy* **2012**, *37*, 4606–4611. [[CrossRef](#)]
19. Chen, P.; Wang, L.K.; Wang, G.; Gao, M.R.; Ge, J.; Yuan, W.J.; Shen, Y.H.; Xie, A.J.; Yu, S.H. Nitrogen-doped nanoporous carbon nanosheets derived from plant biomass: An efficient catalyst for oxygen reduction reaction. *Energy Environ. Sci.* **2014**, *7*, 4095–4103. [[CrossRef](#)]
20. Zhang, H.; Wang, Y.; Wang, D.; Li, Y.; Liu, X.; Liu, P.; Yang, H.; An, T.; Tang, Z.; Zhao, H. Hydrothermal transformation of dried grass into graphitic carbon-based high performance electrocatalyst for oxygen reduction reaction. *Small* **2014**, *10*, 3371–3378. [[CrossRef](#)] [[PubMed](#)]
21. Li, W.; Yue, Z.; Wang, C.; Zhang, W.; Liu, G. An absolutely green approach to fabricate carbon nanodots from soya bean grounds. *RSC Adv.* **2013**, *3*, 20662–20665. [[CrossRef](#)]
22. Guo, C.Z.; Liao, W.L.; Chen, C.G. Design of a non-precious metal electrocatalyst for alkaline electrolyte oxygen reduction by using soybean biomass as the nitrogen source of electrocatalytically active center structures. *J. Power Sour.* **2014**, *269*, 841–847. [[CrossRef](#)]
23. Primo, A.; Atienzar, P.; Sanchez, E.; Delgado, J.M.; García, H. From biomass wastes to large-area, high-quality, N-doped graphene: Catalyst-free carbonization of chitosan coatings on arbitrary substrates. *Chem. Commun.* **2012**, *48*, 9254–9256. [[CrossRef](#)] [[PubMed](#)]
24. Zhao, L.; Baccile, N.; Gross, S.; Zhang, Y.; Wei, W.; Sun, Y.; Antonietti, M.; Titirici, M.M. Sustainable nitrogen-doped carbonaceous materials from biomass derivatives. *Carbon* **2010**, *48*, 3778–3787. [[CrossRef](#)]
25. Liu, S.; Tian, J.; Wang, L.; Zhang, Y.; Qin, X.; Luo, Y.; Asiri, A.M.; Al-Youbi, A.O.; Sun, X. Hydrothermal treatment of grass: A low-cost, green route to nitrogen-doped, carbon-rich, photoluminescent polymer nanodots as an effective fluorescent sensing platform for label-free detection of Cu (II) ions. *Adv. Mater.* **2012**, *24*, 2037–2041. [[CrossRef](#)] [[PubMed](#)]
26. Ma, Z.; Guo, C.; Yin, Y.; Zhang, Y.; Wu, H.; Chen, C. The use of cheap polyaniline and melamine co-modified carbon nanotubes as active and stable catalysts for oxygen reduction reaction in alkaline medium. *Electrochim. Acta* **2015**, *160*, 357–362. [[CrossRef](#)]
27. Paraknowitsch, J.P.; Thomas, A.; Antonietti, M. A zero-emission fuel cell that uses carbonaceous colloids from biomass waste as fuel source. *Chem. Sus. Chem.* **2010**, *3*, 223–225. [[CrossRef](#)] [[PubMed](#)]
28. Lv, G.; Cui, L.; Wu, Y.; Liu, Y.; Pu, T.; He, X. A novel cobalt tetranitrophthalocyanine/graphene composite assembled by an *in situ* solvothermal synthesis method as a highly efficient electrocatalyst for the oxygen reduction reaction in alkaline medium. *Phys. Chem. Chem. Phys.* **2013**, *15*, 13093–13100. [[CrossRef](#)] [[PubMed](#)]
29. Yu, X.; Ye, S. Recent advances in activity and durability enhancement of Pt/C catalytic cathode in PEMFC: Part II: Degradation mechanism and durability enhancement of carbon supported platinum catalyst. *J. Power Sour.* **2007**, *172*, 145–154. [[CrossRef](#)]
30. Chen, P.; Yang, J.J.; Li, S.S.; Wang, Z.; Xiao, T.Y.; Qian, Y.H.; Yu, S.H. Hydrothermal synthesis of macroscopic nitrogen-doped graphene hydrogels for ultrafast supercapacitor. *Nano Energy* **2013**, *2*, 249–256. [[CrossRef](#)]
31. Ma, Y.; Wang, H.; Feng, H.; Ji, S.; Mao, X.; Wang, R. Three-dimensional iron, nitrogen-doped carbon foams as efficient electrocatalysts for oxygen reduction reaction in alkaline solution. *Electrochim. Acta* **2014**, *142*, 317–323. [[CrossRef](#)]
32. Serov, A.; Artyushkova, K.; Andersen, N.I.; Stariha, S.; Atanassov, P. Original mechanochemical synthesis of non-platinum group metals oxygen reduction reaction catalysts assisted by sacrificial support method. *Electrochim. Acta* **2015**. in press. [[CrossRef](#)]
33. Moon, J.S.; Lee, Y.W.; Han, S.B.; Kwak, D.H.; Lee, K.H.; Park, A.R.; Sohn, J.I.; Cha, S.N.; Park, K.W. Iron–nitrogen-doped mesoporous tungsten carbide nanostructures as oxygen reduction electrocatalysts. *Phys. Chem. Chem. Phys.* **2014**, *16*, 14644–14650. [[CrossRef](#)] [[PubMed](#)]
34. Serov, A.; Tylus, U.; Artyushkova, K.; Mukerjee, S.; Atanassov, P. Mechanistic studies of oxygen reduction on Fe-PEI derived non-PGM electrocatalysts. *Appl. Catal. B Environ.* **2014**, *150*, 179–186. [[CrossRef](#)]
35. Singh, D.; Soykal, I.I.; Tian, J.; Deak, D.; King, J.; Miller, J.T.; Ozkan, U.S. *In situ* characterization of the growth of CN_x carbon nano-structures as oxygen reduction reaction catalysts. *J. Catal.* **2013**, *304*, 100–111. [[CrossRef](#)]
36. Yang, S.Y.; Chang, K.H.; Huang, Y.L.; Lee, Y.F.; Tien, H.W.; Li, S.M.; Lee, Y.H.; Liu, C.H.; Ma, C.C.M.; Hu, C.C. A powerful approach to fabricate nitrogen-doped graphene sheets with high specific surface area. *Electrochem. Commun.* **2012**, *14*, 39–42. [[CrossRef](#)]

37. Chen, S.; Bi, J.; Zhao, Y.; Yang, L.; Zhang, C.; Ma, Y.; Wu, Q.; Wang, X.; Hu, Z. Nitrogen-doped carbon nanocages as efficient metal-free electrocatalysts for oxygen reduction reaction. *Adv. Mater.* **2012**, *24*, 5593–5597. [[CrossRef](#)] [[PubMed](#)]



© 2015 by the authors; licensee MDPI, Basel, Switzerland. This article is an open access article distributed under the terms and conditions of the Creative Commons by Attribution (CC-BY) license (<http://creativecommons.org/licenses/by/4.0/>).